Int. J. Heat Mass Transfer. Vol. 33, No. 5, pp. 887–899, 1990
Printed in Great Britain

0017–9310/90 $3.00 + 0.00

Natural convection melting of a frozen porous medium

S. CHELLAIAH† and R. VISKANTA
School of Mechanical Engineering, Purdue University, West Lafayette, IN 47907, U.S.A.

(*Received* 18 *October* 1988 *and in final form* 18 *July* 1989)

Abstract—Melting of an ice-porous media (glass beads) system contained in a rectangular test cell has been studied both experimentally and numerically in order to examine the effects of natural convection and density inversion of water in the melt region. When the superheat across the liquid region is small the flow in the porous media is weak and the interface is almost planar. For larger superheats, the strength of natural convection flow, the interface velocity and shape are all found to depend on the imposed temperature difference and the permeability of the porous medium. The measured temperature distributions are compared with predictions of a numerical model that considers both conduction in the solid and natural convection in the liquid regions. The model is based on volumetric averaging of the macroscopic transport equations, with phase change assumed to occur volumetrically over a small temperature range. Both Brinkman and Forchheimer extensions are added to the Darcy equations. The effect of density inversion of water on the fluid flow and heat transfer is modeled. Reasonably good agreement is found between the experimental data and numerical predictions. The numerical and experimental results establish conclusively that natural convection in the melt region causes the front shape to become nonplanar and increases the melting rate.

INTRODUCTION

SOLID/liquid phase change in saturated porous media occurs in a wide variety of systems in nature and engineering. Applications such as freezing and thawing of soils [1], artificial freezing of ground as a structural support and as a water barrier for construction and mining purposes [2], excavation of frozen soil [3], latent heat-of-fusion energy storage [4], heat transfer in soil around the heat exchanger coils of a ground based heat pump [5, 6], metallurgy [7] and other applications have been discussed at a recent International Symposium on Cold Region Heat Transfer [8]. Despite these varied and many applications, relatively very little attention has been given to the study of solid/liquid phase change of liquid saturated porous media [9]. The related problem of natural convection in porous media in the absence of phase change has been investigated both experimentally and numerically by many researchers and reviews are available [10, 11].

There have been a number of theoretical [2, 12, 13] and experimental [14–17] studies concerned with melting of frozen porous media. Goldstein and Reid [12] studied theoretically thawing of frozen porous media using a mapping technique based on the theory of complex variables by solving the energy equation in the frozen region without knowing the shape of the frozen region. Thawing of soil using electrical heating [13] and microwave energy [3] have been investigated. Both finite element and boundary integral methods were used to model thawing of frozen soil in the absence of convection [14]. Melting of a porous matrix–ice system contained in a cylindrical capsule was studied using a heat conduction based model [15]. The melting of ice around a horizontal tube embedded in a porous matrix (glass beads) has been investigated by Okada and Fukamoto [16]. Melting of a solidified gallium–glass beads system from a vertical wall has been studied numerically employing a two-dimensional enthalpy based model [17]. It was conclusively established both theoretically and experimentally [15–17] that natural convection in the liquid region considerably influences the shape and the motion of the melting front.

This paper reports on an experimental and theoretical study of melting of a glass beads–ice system. Melting of frozen ground is of particular interest because of numerous geophysical and engineering applications [2]. Glass beads were selected as the porous matrix because the thermophysical properties of glass are similar to those of sand, and well characterized uniform size beads were chosen to enable modeling of the transport processes in both the liquid and frozen regions. Melting of a glass beads–ice system contained in a rectangular test cell heated from one of the vertical walls was studied. This is a fundamental geometry which is amenable to mathematical modeling of both natural convection in the liquid region and of the density inversion of water which occurs at 3.98°C. The macroscopic transport equations, volumetrically averaged, with phase change assumed to occur volumetrically over a small tem-

† Present address: Department of Mechanical Engineering, Florida International University, University Park, Miami, FL 33199, U.S.A.

NOMENCLATURE

A	aspect ratio, H/L
C	Forchheimer's constant, 0.55
c	specific heat [J kg^{-1} K^{-1}]
Da	Darcy number, K/L^2
d	mean bead diameter [mm]
$\mathbf{g}$	gravitational acceleration [m s^{-2}]
Δh_f	latent heat of fusion [J kg^{-1}]
H	height of liquid level [m]
K	permeability [m^2]
k	thermal conductivity [W m^{-1} K^{-1}]
L	length of cavity [m]
Ra^*	Rayleigh number for a porous medium, $g\omega KL(T_h-T_f)^q/\nu_l\alpha_l$
S	subcooling parameter, $c_s(T_f-T_c)/\Delta h_f$
s	interface position from hot wall [m]
Ste	Stefan number, $c_l(T_h-T_f)/\Delta h_f$
T	temperature [K]
t	time [s]
$\mathbf{u}$	velocity vector, $\mathbf{i}u+\mathbf{j}v$
u	velocity component in the x-direction [m s^{-1}]
V	volume [m^3]
v	velocity component in the y-direction [m s^{-1}]
x	horizontal from hot wall, see Fig. 1 [m]
y	vertical coordinate, see Fig. 1 [m].

Greek symbols

α	thermal diffusivity, $k/\rho c$ [m^2 s^{-1}]
β	coefficient of thermal expansion [K^{-1}]
γ	volume fraction of liquid phase change material (PCM) in V_f, V_l/V_f
δ	volume fraction of liquid PCM in the volume element, $V_l/V=\phi\gamma$
ζ	dimensionless interface position, s/L
η	dimensionless vertical coordinate, y/L
θ	dimensionless temperature, $(T-T_c)/(T_h-T_c)$
μ	dynamic viscosity [N s m^{-2}]
ν	kinematic viscosity [m^2 s^{-1}]
ξ	dimensionless horizontal coordinate, x/L
τ	dimensionless time, $t\alpha_l/L^2$
ϕ	porosity or volume fraction of PCM in the volume element, V_f/V.

Subscripts

eff	effective
f	fluid
c	cold
h	hot
l	liquid
m	maximum
p	porous matrix
ref	reference
s	solid.

perature range [17] were used. In the liquid region, both the Brinkman and Forchheimer extensions were included in the Darcy equation. The effect of density inversion of water on the fluid flow and heat transfer were also modeled. The experimental temperature data and the deduced solid/liquid interface positions were compared with the corresponding predictions of the numerical model.

EXPERIMENTS

Test cell

Melting experiments were performed in a rectangular test cell with inner dimensions of 205 mm in length, 203 mm in height and 127 mm in width. The top, bottom, front and back sides were made of Plexiglass (12.5 mm thick). Two Plexiglass plates separated by a 6 mm air gap were used on the front and back of the test cell to minimize the effect of heat gains and condensation of moisture (Fig. 1). A 7.5 mm wide and 172 mm long slot was cut in the top plate. The test cell was filled with water and glass beads through this opening. A lid snugly fits into this slot. Two 11 mm diameter holes were cut on this lid to bring out the thermocouple wires.

Two copper heat exchangers with milled passages for flow of coolant constituted the left and right endwalls of the test cell. The flow passages inside the heat exchanger were milled in such a way that the maximum temperature variation along the surface of the heat exchanger was within ± 0.2°C. Six thermocouples were placed along the surface of the heat exchanger to check the uniformity of the temperature along the faces. The entire test cell was covered with 50 mm thick Styrofoam on all sides. The test cell was placed on an iron plate fitted with leveling screws.

Two thermocouple rakes with 21 copper–constantan thermocouples in each and supported on two half rings epoxied on to the surface of the heat exchangers were located at 1/3 and 2/3 height from the bottom and along the centerplane of the test cell. This was a compromise between the resolution desired and the disturbance of the system by additional rakes. The temperature readings were automatically recorded at preset time intervals using a data logger connected to a VAX microcomputer.

Test materials and procedure

Glass beads having diameters of 2.85, 6.0 and 12.5 mm constituted the porous matrix. The properties used for the numerical study were those of glass with a chemical composition as close as could be obtained

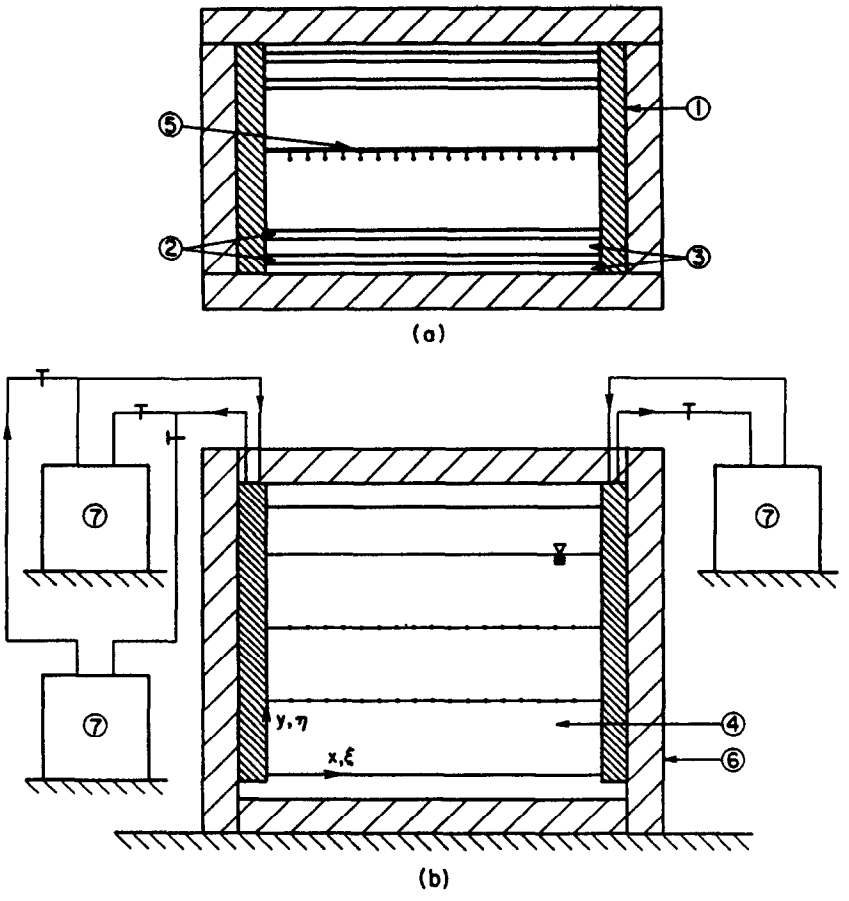

FIG. 1. Schematic of test arrangement.

to that of the beads used in this study [18]. The test cell was filled with glass beads with rakes kept in position and was shaken manually to ensure close and random packing. Once distilled and degasified water was carefully siphoned into the test cell without introducing air bubbles into the system. A mixture of ethyl alcohol and water was circulated through the heat exchangers from two constant-temperature baths and the porous matrix and water were allowed to cool to the desired initial temperature.

The melting was initiated by switching one of the constant temperature baths to a third one that was already heated separately to the desired temperature. The natural convection flow in the porous media was observed in parallel flow visualization experiments.

The heat exchangers have a finite thermal capacity, and hence a finite time is needed for them to reach a steady-state temperature. This heat-up transient is further influenced by the heat absorbed during melting. The heat exchanger temperature increases very sharply during a brief initial period (the duration of which depends on the experimental conditions) and remains constant afterwards. The duration of this heat-up transient is small, less than 1% of the duration (about 5–8 h) of the experiment. Likewise, the variation of wall temperature along the height of the wall is about 5% (1°C) (for the first 2–3 min) and drops to less than 1% (0.2°C) of the average wall temperature. The variation of the wall temperature along the width of the heat exchangers is also of about the same magnitude.

ANALYSIS

The physical system modeled consists of a rectangular cavity with two vertical walls maintained at two different temperatures and the top and bottom surfaces insulated. The cavity is filled with a mixture of water and glass beads and the entire system is first frozen. At time, $t = 0$, a uniform temperature greater than the fusion temperature is imposed on the left wall. Melting is initiated at this wall and the interface moves from left to right (Fig. 1). The following simplifying assumptions are made in the analysis: (1) the porous medium is isotropic, homogeneous and has uniform porosity; (2) the porous matrix and the phase change materials are in local thermal equilibrium; (3) the flow is two-dimensional, laminar and incompressible; (4) the volume change due to melting is negligible; (5) the phase change medium has a definite fusion temperature; (6) the porous matrix and the solid are stationary; (7) all thermophysical properties

are independent of temperature; and (8) the momentum flux due to the interface motion is negligible.

The complicated geometry, heat transfer and the flow pattern in the system prohibit the solution of the governing equations at the microscopic level. Hence, the equations are averaged over a small volume element. In general, in such a volume element, there can be both solid and liquid phases along with the porous matrix. In the melt region, the material is entirely liquid and $\gamma = 1, \delta = \phi$ and in the solid region, $\gamma = \delta = 0$. Fuller details of the development of the volume averaged governing equations can be found in the literature [10, 11]. Even though the phase change is assumed to occur at a discrete temperature, in a volume element containing both the porous matrix as well as the solid and liquid, the average temperature may be slightly higher or lower than T_f. Hence, it is assumed that both solid and liquid may exist simultaneously in a volume element, if its temperature lies within a small temperature difference ΔT, on either side of the fusion temperature. A more detailed discussion of the model is given elsewhere [17]. The two-dimensional conservation of mass, momentum and energy equations for melting of liquid saturated porous media are, respectively,

$$\nabla \cdot \mathbf{u} = 0 \tag{1}$$

$$\frac{\rho_l}{\delta}\frac{\partial \mathbf{u}}{\partial t} + \frac{\rho_l}{\delta^2}(\mathbf{u}\cdot\nabla)\mathbf{u} = -\nabla p + \frac{\mu_l}{\delta}\nabla^2\mathbf{u} - \left[\frac{\mu_l}{K} + \frac{\rho_l C}{K^{1/2}}|\mathbf{u}|\right]\mathbf{u} - \rho\mathbf{g} \tag{2}$$

$$\overline{\rho c}\frac{\partial T}{\partial t} + \rho_l c_l(\mathbf{u}\cdot\nabla T) = \nabla\cdot(k_{\text{eff}}\nabla T) - \phi\rho_l\Delta h_f\frac{\partial \gamma}{\partial t}. \tag{3}$$

The momentum balance takes into account the unsteady term, Forchheimer's and Brinkman's extensions to the Darcy equations. Equation (3) is the volume averaged energy equation for the general control volume containing the porous medium solid–liquid mixture. With the velocity set to zero ($\mathbf{u} = 0$), equation (3) is also appropriate for the frozen region.

The boundary conditions for temperature are

$$T = T_h \quad \text{at} \quad x = 0 \quad \text{for all } y$$
$$T = T_c \quad \text{at} \quad x = L \quad \text{for all } y \tag{4}$$

$$\frac{\partial T}{\partial y} = 0 \text{ at } y = 0 \text{ and at } y = H \text{ for all } x. \tag{5}$$

There is no slip at the walls. At the free surface the boundary conditions for the velocity are

$$\frac{\partial u}{\partial y} = v = 0 \quad \text{at} \quad y = H \quad \text{for} \quad 0 < x < s. \tag{6}$$

For $t < 0$, $u = v = 0$ and $T = T_c$.

The buoyancy force is $\rho\mathbf{g}$, with ρ denoting the local density, corresponding to the local temperature. For fluids having a linear density–temperature relationship the usual simplification of the buoyancy term can be carried out. But the density–temperature relationship for water is nonlinear and it attains a maximum value at 3.98°C. Several equations of state (second, third and fourth degree polynomials) [19–21] have been proposed for the density of water as a function of temperature. In this study we use the approximation for density of water suggested by Gebhart and Mollendorf [19]

$$\rho = \rho_m(1 - \omega|T - T_m|^q) \tag{7}$$

where $\omega = 9.2972 \times 10^{-6}(°C)^{-q}$, and $q = 1.8948$.

The mean thermal capacitance of the mixture ($\overline{\rho c}$) is defined by

$$\overline{\rho c} = \phi[\gamma\rho_l c_l + (1-\gamma)\rho_s c_s] + (1-\phi)\rho_p c_p. \tag{8}$$

The effective conductivity of the porous media was calculated using the Veinberg model [22], for it was found to give the best comparison (as compared to different models) between predictions and measured temperatures and interface location for melting of a glass beads–ice system initially at saturated temperature [15]. It should be stressed that the effective thermal conductivity of liquid saturated porous media under static conditions was assumed to be the same as that for a transient system with a flowing fluid in which dispersion effects may be present.

The value of the permeability, K, was calculated from the Kozeny–Carman equation

$$K = \frac{d^2\phi^3}{175(1-\phi)^2}. \tag{9}$$

The value of the inertia coefficient C in Forchheimer's extension was found to be nearly constant [24], and a value of 0.55 was used in the calculations.

The model equations were solved using the SIMPLER algorithm [25] and computational details are given as in an earlier paper [17]. After conducting numerical sensitivity studies with different grids and time steps, a uniform grid of 26×26 nodal points was chosen as a compromise between cost and accuracy.

RESULTS AND DISCUSSION

Experimental results

Experimental conditions. A number of experiments with several different size beads and several different superheats were conducted. For space limitations, only a few of them are discussed here. Additional results are presented elsewhere [18]. The experimental conditions are summarized in Table 1. The porosity was calculated as the ratio of the volume of water siphoned into the test cell to the volume of the test cell. All properties of ice, water and glass were taken at the fusion temperature 0°C. Since water undergoes a density inversion, the Rayleigh number was calculated as suggested in the literature [21].

From Table 1, it is seen that the porosity ϕ varies with bead size. For a system of infinite volume, ran-

Table 1. Summary of experimental conditions for melting of ice–glass beads system

Exp.	d (mm)	T_h (°C)	T_c (°C)	ϕ	$K\times10^9$ (m²)	$Da\times10^7$	S	Ste	Ra^*
1	12.5	4.0	−0.43	0.412	180.6	42.9	0.0	0.051	188.6
2	12.5	7.6	−0.95	0.412	180.6	42.9	0.0	0.100	628.5
3	12.5	18.9	−0.83	0.412	180.6	42.9	0.0	0.240	3579.8
4	12.5	24.8	−0.39	0.412	180.6	42.9	0.0	0.314	5984.0
5	12.5	29.1	−0.52	0.412	180.6	42.9	0.0	0.368	8075.2
6	6.0	9.2	−0.89	0.396	35.0	8.3	0.0	0.117	184.0
7	6.0	20.7	−0.85	0.396	35.0	8.3	0.0	0.262	852.7
8	6.0	30.3	−0.35	0.396	35.0	8.3	0.0	0.385	1767.9
9	6.0	20.3	−2.79	0.396	35.0	8.3	0.018	0.257	821.0
10	6.0	29.5	−4.53	0.396	35.0	8.3	0.029	0.374	1682.0
11	2.85	29.7	−0.59	0.377	6.4	1.5	0.0	0.377	323.3
12	2.85	30.5	−3.33	0.377	6.4	1.5	0.021	0.387	350.0
13	2.85	21.3	−4.68	0.377	6.4	1.5	0.03	0.269	171.4

domly packed with uniform size spheres, the porosity is constant and is independent of the bead size [26]. Since the test cells used in experiments are finite in size, there is a considerable variation of porosity near the walls, especially with the larger size beads. With 2.85 mm beads, the porosity is close to the theoretically expected value for randomly packed beds. The porosities of the system with the two smaller size beads are nearly the same, because there is not much difference in their sizes to affect the packing density. But, with the larger size beads the porosity is higher.

There are a large number of parameters which affect the transport processes during the melting of frozen porous media. The parameters include the Stefan number (Ste), the Darcy number (Da), the Rayleigh number for a porous medium (Ra^*), the subcooling parameter (S), and the aspect ratio (A). Some of these parameters are not independent of each other. For example, the temperature difference $(T_h - T_f)$ appears in both the definitions of the Stefan and the Rayleigh numbers. As a consequence, it is difficult to be comprehensive. Some typical results are presented in this paper, and additional results are available elsewhere [18].

Effect of bead size. The bead size directly influences the permeability, equation (9), and hence the Darcy number of the system. The effect of bead size on the melting process can be investigated by comparing results of experiments 5, 8, and 11 that have nearly identical experimental conditions. The small variations in porosity with bead size cause changes in permeability and hence also in Rayleigh numbers.

The temperature distributions for experiment 5, at different times as recorded by the top and bottom thermocouple rakes, are presented in Fig. 2. At the start of the experiment, the ice is nearly at the fusion temperature. The average initial temperature is −0.52°C. Since the test cell is 20.5 cm wide, even after circulating coolant through the heat exchangers for 24 h, to bring the system as close to 0°C as possible, the ice near the two walls is at −0.05°C, whereas in the central region of the test cell the ice remains at about −0.8°C. Further heating of the two walls to raise the temperature in the central region close to 0°C would melt the ice near the walls. Therefore, the average initial temperature could not be raised closer to 0°C.

Initially the melting is solely due to heat transfer by conduction, and the interface is planar (i.e. the melt thickness does not vary along the vertical direction). With the progress of melting, the melt region in the test cell increases. At early times, the aspect ratio of the melt region (H/s, where s is the melt thickness) is very high and it gradually decreases. In the case of thermal buoyancy-driven convection in a rectangular cavity filled with a liquid saturated porous medium, the boundary layers form when the Darcy-modified Rayleigh number based on the height of the cavity exceeds a limit given by [27]

$$(Ra^*)^{1/2} > A \tag{10}$$

where

$$Ra^* = g\beta KH(T_h - T_c)/(\alpha\nu_f) \tag{11}$$

and

$$\alpha = k_{eff}/(\rho c_f). \tag{12}$$

Studies to show the corresponding limits for a water saturated porous medium in the presence of density inversion could not be found. The thermal expansion coefficient of water varies from -67.5×10^{-6} to 303.8×10^{-6} °C^{-1} [28] for the temperature range (0–30°C) encountered in the experiments. Using the value of β at the average of the hot wall and interface temperatures (the two bounding temperatures driving natural convection for experiment 5), one finds that $Ra^* = 1030$. Accordingly, the vertical boundary layers develop when

$$(Ra^*)^{1/2} = 32 > H/s \tag{13}$$

where s is the instantaneous melt thickness. From Fig. 2, it is seen that the instantaneous aspect ratio based on the melt thickness ($K = 15$ cm, $s = 2$ cm and $A = 7.5$) at $t = 0.5$ h, is small so that equation (13) is

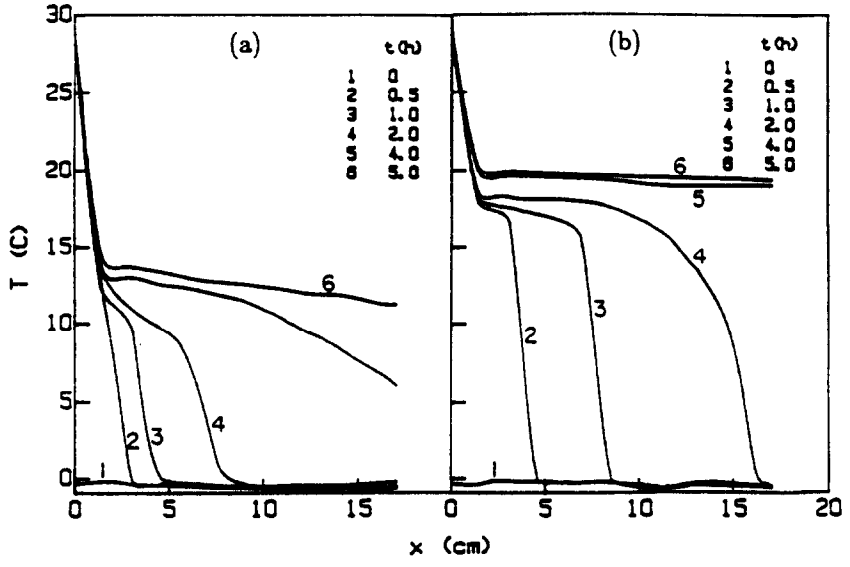

FIG. 2. Temperature distribution at different times for experiment 5 ($d = 12.5$ mm, $\phi = 0.412$, $S = 0$, $Ste = 0.368$, $Ra^* = 8075.2$): (a) bottom rake, $\eta = 0.333$; (b) top rake, $\eta = 0.667$.

satisfied, and the formation of vertical boundary layers is expected. The time at which the boundary layers stop growing was determined [27] as

$$t = \frac{(\rho c)_{\text{eff}} H^2}{(\rho c)_f \alpha \, Ra^*}. \tag{14}$$

It is evident from Fig. 2 that the boundary layer thickness at different times is the same as that at $t = 0.5$ h. The temperature distributions in the boundary layer qualitatively compare well with their predictions. Quantitative comparison is not possible, because the experimental conditions are different.

The temperature distributions reveal that the rate of melting along the top rake is faster than that along the bottom. This is similar to that observed during melting of pure materials in the absence of a porous matrix [29]. The temperature difference between the hot wall and the interface drives the natural convection flow in the liquid. The water near the hot wall rises and turns towards the interface. As the water is cooled, its density attains a maximum value at 4°C, and descends along the 4°C isothermal surface forming a clockwise rotating cell. The water in the region bounded by 0–4°C isotherms has only a small temperature potential to drive the flow and hence is overpowered by the clockwise circulating flow. The influence of convection can be seen (from the difference in melting rates at the two heights) as early as 0.5 h after the start of melting. At $t = 1$ h, the melted region was 8.5 cm wide along the top rake and 4.5 cm wide along the bottom rake. Along the top rake, there is a steep temperature decrease of about 10°C in the 2 cm thick region near the hot wall. This distribution qualitatively compares well with the predictions of free convection in a porous layer adjacent to a vertical impermeable surface [11].

At the end of a 4 h time period, all the ice had melted, except for a small amount near the bottom of the cold wall. After 5 h, the temperature distribution along the top rake was practically uniform except for the temperature drop near the hot wall. Strong convective flow in the top region has effectively eliminated the temperature variation. There is a temperature drop of about 8°C in the 2 cm melt region near the hot wall, and then the temperature remains constant up to the last thermocouple (3 cm from the cold wall); however, along the bottom rake (Fig. 2(a)), a temperature gradient is still evident in the melt region after the 15°C drop in the 2 cm region near the hot wall.

The temperature distributions along the two rakes for the intermediate size beads (experiment 8, $Da = 8.3 \times 10^{-7}$) are between those for experiments 5 and 11; therefore, they are not shown for the case of brevity but are available elsewhere [18]. The temperature distributions at different times along the top and bottom rakes for experiment 11 are shown in Fig. 3. They reveal that the rate of melting along the top of the cell is higher than that along the bottom, and the convective flow is weaker than in experiment 5. Therefore, even after 1 h there is only a small difference in the melting rates at the two heights. Only at later times the effect of convection is seen to produce higher melting rates along the top than along the bottom.

A comparison of results presented in Figs. 2 and 3 shows that the difference in temperature distributions along the two rakes at $t = 5$ or 6 h into the experiment, decreases with decrease in bead size. In other words, the convective flow is weaker with smaller size beads and melting is dominated by conduction for longer times. The rates of melting along the two rakes for

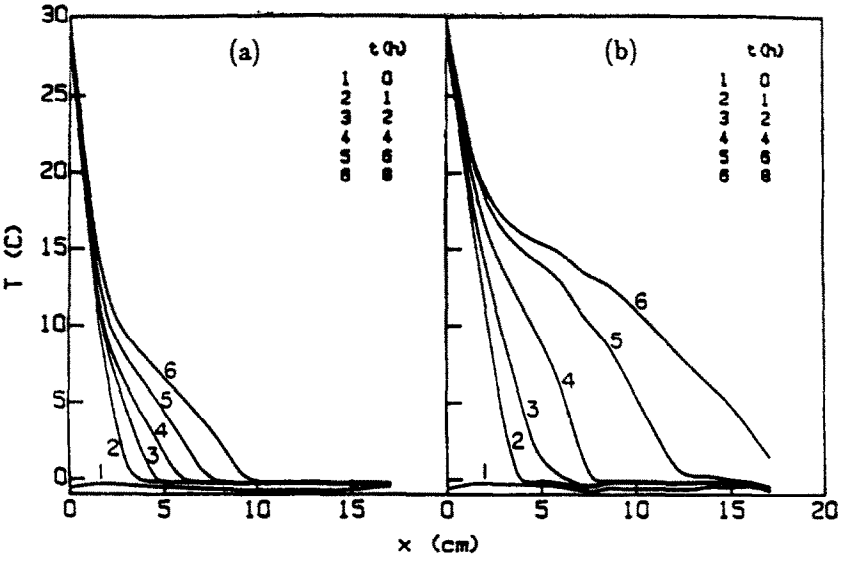

FIG. 3. Temperature distribution at different times for experiment 11 ($d = 2.85$ mm, $\phi = 0.377$, $S = 0.377$, $Ra^* = 323.3$): (a) bottom rake, $\eta = 0.333$; (b) top rake, $\eta = 0.667$.

experiments 5, 8 and 11 are shown in Fig. 4. There is more melting at the top than along the bottom rake. The rate of melting is highest for experiment 5 (strongest flow) and smallest for experiment 11 (weakest flow). This is due to the thermal buoyancy driven convection in the melt. The results are consistent with the theoretical predictions of natural convection in porous media in the absence of melting and motion of the phase change boundary [27].

Effect of Rayleigh number. For a fixed test cell (i.e. constant L) and fixed bead size (i.e. constant permeability, K), changes in hot wall temperature produce changes in Rayleigh number Ra^*. Therefore, the effect of Rayleigh number (with Darcy number and aspect ratio of the test cell kept fixed) is the same as the effect of hot wall temperature. This effect can be delineated by comparing the interface locations (Fig. 5) of experiments 1, 2, 4 and 5 that have Rayleigh numbers of 188.6, 628.5, 3579.8 and 8075.2, respectively.

In experiment 1, the Rayleigh number is so small that the time taken for the onset of convection is the longest. The melting is controlled by conduction as revealed by the equal rates of melting along the two rakes up to about 7 h (Fig. 5). Then, after convection sets in, the melting rates differ at the two heights, but

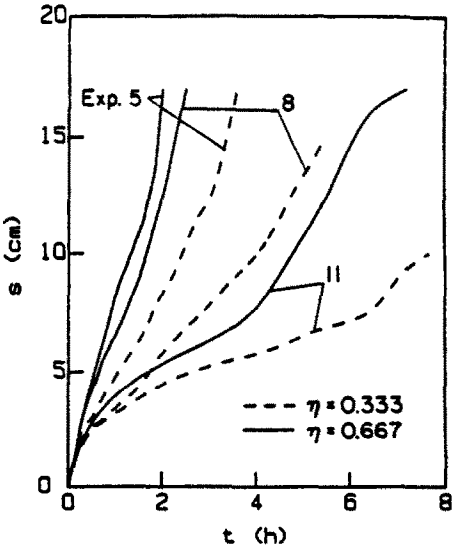

FIG. 4. Effect of bead size on the rate of melting for experiments 5 ($d = 12.5$ mm), 8 ($d = 6.0$ mm), and 11 ($d = 2.85$ mm).

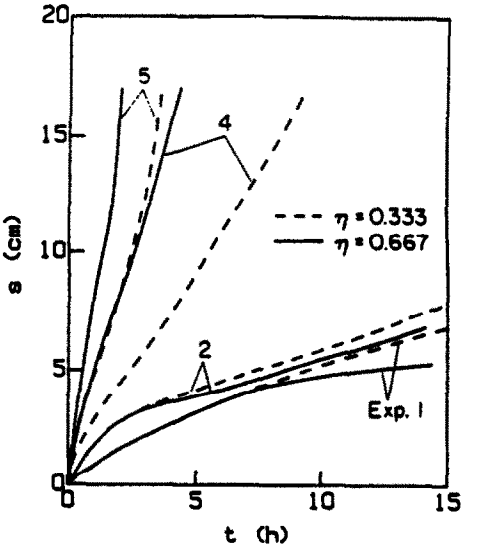

FIG. 5. Effect of Rayleigh number on the rate of melting for experiments 1 ($Ra^* = 188.6$), 2 ($Ra^* = 628.5$), 4 ($Ra^* = 5984.0$), and 5 ($Ra^* = 8075.2$).

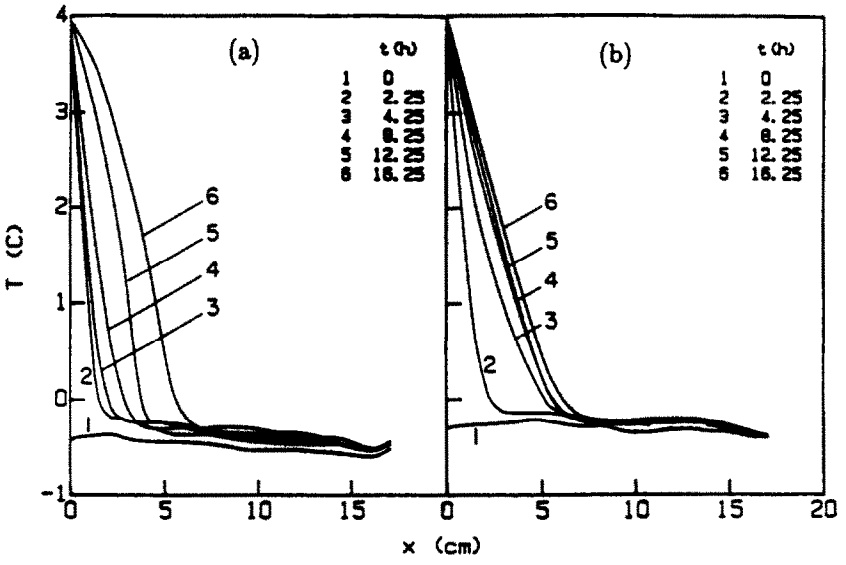

FIG. 6. Temperature distribution at different times for experiment 1 ($d = 12.5$ mm, $\phi = 0.412$, $S = 0$, $Ste = 0.051$, $Ra^* = 188.6$): (a) bottom rake, $\eta = 0.333$; (b) top rake, $\eta = 0.667$.

as the hot wall temperature is just equal to the density inversion point of water, there is more melting observed along the bottom rake. As T_h is further increased, the Rayleigh numbers increase and convection sets in at early times as seen from the difference in the rates of melting along the two rakes (Fig. 5). With increasing T_h, the clockwise flow in the region bounded by the hot wall and the 4°C isotherm becomes stronger and gradually overpowers the counterclockwise flow between the interface and the 4°C isotherm. This produces faster melting along the top than at the bottom as in the case of pure materials [29]. With an increase in Rayleigh number, the convective flow becomes stronger, causing larger differences between the melting rates along the two rakes even at early times in the experiment. This trend is characteristic of melting experiments in the absence of a porous matrix [29].

With an increase in the Rayleigh number, a boundary layer begins to form along the hot wall. It should be noted that the Rayleigh numbers are based on the width of the test cell. This characteristic length is not really meaningful, because as melting progresses the melt region increases in size and the aspect ratio also continuously decreases. Unfortunately, alternate characteristic length scales have not been proposed in the literature for moving boundary problems. By comparing the temperature distributions for experiments 1 (Fig. 6) and 5 (Fig. 2), the effect of stronger convective flow driven by higher thermal buoyancy forces can be seen clearly. In experiment 1, boundary layers are not evident and the temperature decreases monotonically, whereas in experiment 5 the boundary layer formation is clearly evident.

Effect of density inversion of water. When buoyancy induced convection takes place in water, if both the hot and cold wall temperatures are below (above) the density inversion point of water, then the density of water in that temperature range $(T_h - T_c)$ increases (decreases) with the increase in temperature. During melting, the phase change front is at the fusion temperature. If the hot wall temperature is above 4°C, then there is a location in the liquid along which water attains its maximum density. The effect of density inversion on the melting process is discussed below by comparing the results of experiments 1 and 5.

The temperature distributions along the two rakes for experiment 1 are shown in Fig. 6. At early times, the temperature in the liquid region decreases monotonically from the hot wall to the interface. This indicates that heat transfer is predominantly by conduction. The temperature difference, $(T_h - T_c) = 4$°C, is small so the convection is very weak. This is evident from Fig. 5, which shows the interface positions at different times along the two rakes. The melting rates are the same along the two rakes up to about $t = 7$ h. Afterwards, the effect of convection is noticeable and melting along the bottom rake is faster than that along the top rake. Water near the interface is lighter than that near the hot wall. Therefore, it rises along the interface, turns left and flows downwards along the hot wall as it is heated. Thus, when the liquid reaches the bottom of the heated wall, it is hotter and causes more melting near the bottom than at the top. This counterclockwise flow is opposite to the clockwise flow observed in melting of common substances in the absence of density inversion [29].

In experiment 5 the hot wall is at a temperature of 29.05°C. The clockwise flow in the region between the wall and the 4°C isotherm is much stronger than the counterclockwise flow in the temperature region 0–4°C. Therefore, the melting process is similar to that of common substances and higher melting rates are observed along the top of the hot wall.

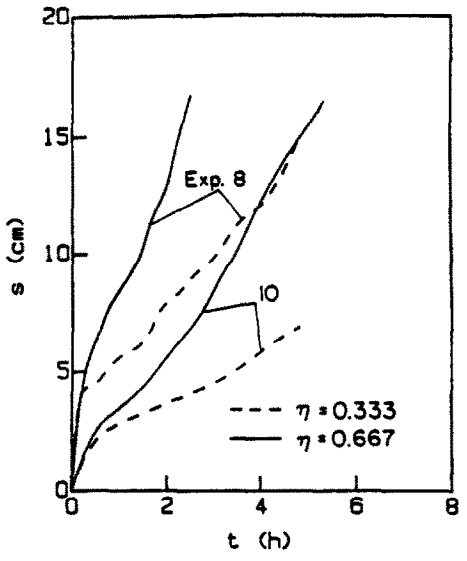

FIG. 7. Effect of subcooling parameter on the rate of melting for experiments 8 ($S = 0$) and 10 ($S = 0.029$).

Effect of solid subcooling. The subcooling parameter, S, is a measure of the amount of sensible heat that must be added to the frozen system to raise its temperature to the fusion temperature. The rates of melting for experiments 8 ($S = 0$) and 10 ($S = 0.029$) are compared in Fig. 7 to show the effect of the solid region subcooling on the melting process. The results show that the subcooling has delayed the initiation of thermal buoyancy driven convective flow in the melt, weakened the flow and slowed down the melting process. A subcooling of $-4.5°C$ ($S = 0.029$) retards the melting process to the extent that at the end of 2 h the melt layer thickness along the top rakes for experiments 8 and 10 are 13 and 5.9 cm, respectively. Along the bottom rake, the respective values are 8 and 3.8 cm.

Numerical simulations of melting

The melting of an ice–glass beads system was numerically simulated using the enthalpy based model described earlier. In order to provide a more critical comparison between model predictions and the experimental data, experiment 13 was selected, because both natural convection flow in the liquid region and heat conduction in the frozen solid region must be accounted for in the analysis. Preliminary simulations were performed, with 26×26, 41×41 and 51×51 grid systems. The computer time and the cost of the simulations were very high for the latter two finer grids. Additionally, extensive grid independence studies could not be conducted due to the high cost and large computer time required. Hence, a 26×26 grid was chosen as a compromise between cost and accuracy. A value of $\Delta\theta = 0.0195$ was used. The time step was kept small [$\tau = 3.13 \times 10^{-6}$ ($t = 1$ s)] during the initial period of simulation when the transients are large and gradually increased to a maximum of $\tau = 1.57 \times 10^{-5}$ ($t = 5$ s). The simulations were terminated when the significant variables (velocities and temperatures) agreed up to three decimal places and the residual mass was less than 10^{-6}. The calculations required about 21 000 s of CPU time on a Cyber 205 supercomputer.

The streamlines and isotherms at $\tau = 0.0226$ ($t = 2$ h) (not shown) already revealed the influence of thermal convection flow on heat transfer and local melting. The isotherms were inclined towards the cold wall near the top indicating more melting at the top than at the bottom. The water near the hot wall is lighter and rises gaining heat as it flows upwards along the hot, left wall. At the free surface the flow turns right and impinges on the interface. It then loses heat, becomes heavier and flows downwards along the interface. This causes more melting at the top than at the bottom as in the case of melting of a pure substance [29].

Even though the water undergoes a density inversion, the water in the region bounded by 0–4°C isotherms has only a small potential to drive the flow and is overpowered by the flow in the region bounded by the hot wall and 4°C isothermal surface. Thus, only one clockwise cell is predicted. The cold wall is at $-4.68°C$, and hence there is a temperature difference of 4.7°C in the solid region bounded by the interface and the cold wall.

Figure 8 shows the streamlines and isotherms at $\tau = 0.068$ ($t = 6$ h). The isotherms clearly reveal a larger liquid region at the top than at the bottom of the test cell. The streamlines are smooth and reveal a single clockwise rotating cell for reasons mentioned above. The absolute values of the stream functions have increased with time indicating larger velocity gradients near the center of the cell. The streamline and isotherms qualitatively agree with those of previous investigators [27, 30, 31] who numerically studied the natural convection in rectangular cavities filled with porous media in the absence of phase change.

The temporal variation of the average Nusselt number at the hot wall is shown in Fig. 9. The average Nusselt number is defined as

$$Nu_{ave} = \frac{-L}{H(T_h - T_f)} \int_0^H \left.\frac{\partial T}{\partial x}\right|_{x=0} dy \qquad (15)$$

using the width of the cavity, L, as the characteristic length. It should be mentioned that the width of the cavity is not the most appropriate choice for the length scale, because the size and shape of the liquid region changes with time. A more appropriate scale for a moving boundary problem could not be found in the literature. The temperature difference used in equation (15) is that between the hot wall and the melt front which drives the convective flow in the liquid. When conduction is the only mode of heat transfer, the heat flux at the hot wall is inversely proportional to the square root of time; therefore, at early times in

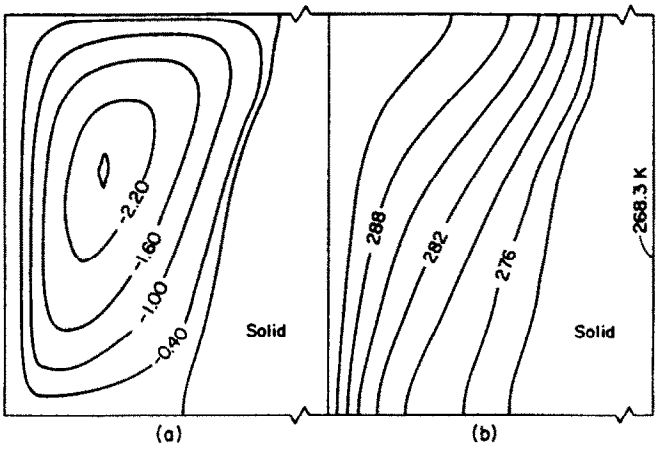

FIG. 8. Predicted flow and temperature fields for experiment 13 at $t = 6$ h ($d = 2.85$ mm, $\phi = 0.377$, $S = 0.03$, $Ste = 0.269$, $Re^* = 171.4$): (a) streamlines (ψ in kg m^{-1} s^{-1}); (b) isotherms (K).

the simulation the heat flux and the Nusselt number are very large. As melting progresses, convection currents set in and the Nusselt number reaches a quasi-steady value. This trend is similar to that observed in ref. [32] for melting of pure substances in the absence of a porous matrix.

Comparison of predicted results with experimental data

A comparison between the predicted and the measured temperature distributions for experiment 13 at different times and along the two different vertical locations is presented in Fig. 10. In general, the agreement between the two results is good, but the temperatures in the liquid region are always overpredicted. Any heat gains from the ambient to the test cell would tend to increase the temperatures not lower them; therefore, the gains can be dismissed as the reason for the discrepancy. Certainly, the porosity and permeability are not uniform within distances of a few ball diameters from the melting front and the hot wall. In the test cell, the porosity varies exponentially from a value of unity at the hot wall to about 0.37 in the region about 3–4 bead diameters away [33]. This translates to higher permeability and lower resistance to fluid flow in this region. Additionally, the viscosity of water decreases by a factor of 1.8 from 1.787×10^{-3} kg s m^{-1} at 0°C to 1.002×10^{-3} kg s m^{-1} at 20°C near the hot wall [28]. These two factors tend to produce steeper temperature gradients near the hot wall. The model has ignored these effects and, therefore, predicts higher temperatures in the liquid near the hot wall. Overall, the agreement between the predicted and measured temperatures in the liquid region is within 5% and that in the solid region is within 1% of the total temperature difference across the test cell. The effect of wall-channeling due to the porosity variation near the wall and the dependence of viscosity of water on temperature are believed to be the important reasons for increasing the temperature gradients near the hot boundary. The predicted temperature gradients based on uniform porosity and permeability are smaller than the measured ones, particularly at later times in the melting process.

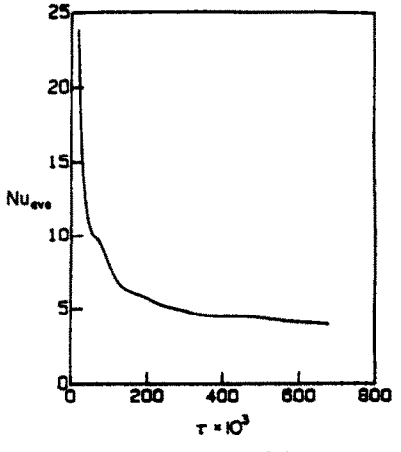

FIG. 9. Predicted timewise variation of the average Nusselt number at the hot wall for conditions of experiment 13 ($d = 2.85$ mm, $\phi = 0.377$, $S = 0.03$, $Ste = 0.269$, $Ra^* = 171.4$).

Figure 11 shows a comparison of the predicted and measured dimensionless interface positions. Along the top rake, there is good agreement between the predictions and the experimental data up to about $\tau = 0.0395$ ($t = 3.5$ h). Afterwards, the model predicts higher melting rates. Along the bottom rake, after about $\tau = 0.0226$ ($t = 2$ h), the model predictions depart from the experimental data. This is because the temperature in the liquid region is predicted to be higher than that measured experimentally. But the model clearly shows that the effect of natural convection is to augment the rate of melting along the top rake.

There are a number of factors which may contribute to the discrepancy between data and predictions and include the following: (1) contraction of the liquid, (2) inappropriate permeability and effective thermal conductivity models for the porous media, (3) precise

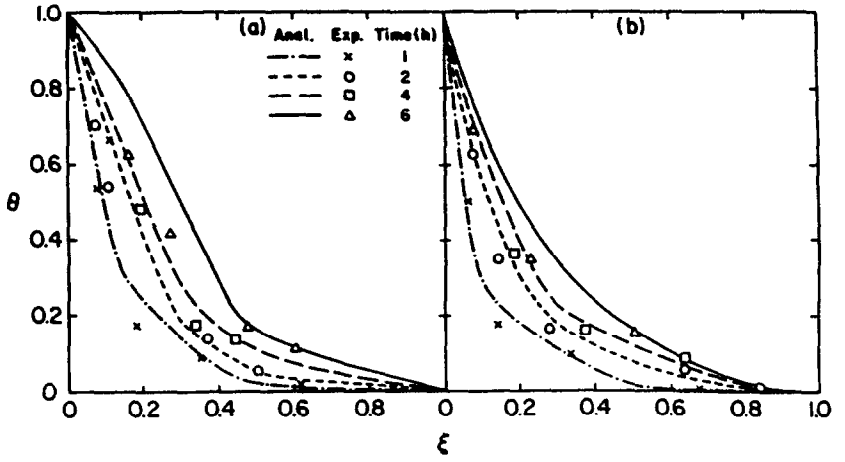

FIG. 10. Comparison of experimental and predicted temperature distributions at different times for experiment 13 ($d = 2.85$ mm, $\phi = 0.377$, $S = 0.03$, $Ste = 0.269$, $Ra^* = 171.4$): (a) top rake, $\eta = 0.667$; (b) bottom rake, $\eta = 0.333$.

location of the interface in the region where both the liquid and solid phases coexist, (4) thermophysical property variation with temperature, and (5) numerical errors due to an insufficiently fine grid. The modeling of the permeability in the liquid region, and in particular in the region where both the liquid and solid are present may not be accurate [17]. The control volumes are relatively large (8.5 mm) to be represented by a node and assigned a single temperature. All of these factors can affect the flow structure, temperature distributions in the solid and liquid regions and alter the melting front shape and motion.

CONCLUSIONS

An experimental and numerical study of melting of a glass beads–ice system has been performed. A number of different experiments using three different size beads and subcoolings have been conducted. The experiments performed have provided conclusive evidence that natural convection in the liquid region causes the melting front to become nonplanar and increases the rate of melting. The intensity of natural convection in the melted region depends on the Rayleigh number of the porous medium Ra^*.

An enthalpy based numerical model that considers both diffusion in the solid and liquid regions and thermal buoyancy driven convection in the liquid has been used to simulate melting of liquid saturated porous media. The numerical predictions were compared with measured temperatures and interface positions, and good correspondence has been found. The possible reasons for the discrepancy between model predictions and the data have been discussed. The computational resources needed to obtain solutions were excessive.

There is a need for flow visualization and nonintrusive diagnostics for temperature and melting front position measurement in porous media, both in the absence and in the presence of phase change. There is also a need for developing efficient, accurate, cost-effective numerical algorithms for solving the model equations for two- and three-dimensional solid/liquid phase change of porous media in the presence of natural convection.

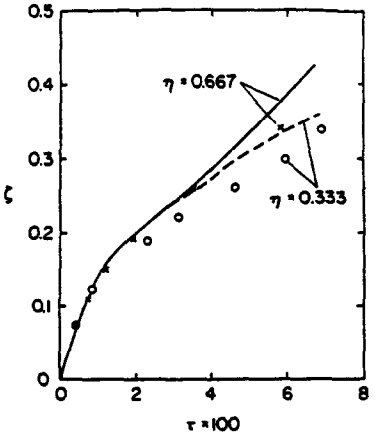

FIG. 11. Comparison of predicted and experimental melt front locations for experiment 13 ($d = 2.85$ mm, $\phi = 0.377$, $S = 0.03$, $Ste = 0.269$, $Ra^* = 171.4$).

Acknowledgements—The work reported in this paper was supported, in part, by the Heat Transfer Program of the National Science Foundation under grant No. CBT-8313573.

REFERENCES

1. V. J. Lunardini, *Heat Transfer in Cold Climates*. Van Nostrand Reinhold, New York (1981).
2. F. J. Sanger, Ground freezing and construction, *ASCE Mech. Found. Div.* **94**, 131–158 (1968).
3. Yu. M. Misnyck, O. B. Shonin, N. I. Raybets and V. S. Petrov, Application of microwave energy for accelerating excavation in frozen soil. In *Final Proc. Fourth*

Int. Conf. on Permafrost, pp. 268–272. National Academy of Sciences Press, Washington, DC (1983).
4. ME Staff, Seasonal thermal energy storage, *Mech. Engng* **105**, 28–34 (1983).
5. P. D. Metz, A simple computer program to model three-dimensional underground heat flow with realistic boundary condition, *J. Sol. Energy Engng* **105**, 42–49 (1983).
6. O. Svec, L. E. Goodrich and J. H. L. Planar, Heat transfer characteristics of ground heat exchangers, *J. Energy Res.* **7**, 263–278 (1983).
7. K. M. Fisher, The effects of fluid flow on the solidification of castings and ingots, *PhysicoChem. Hydrodyn.* **2**, 311–326 (1981).
8. K. C. Cheng, V. J. Lunardini and N. Seki, *Proc. 1987 Int. Symp. on Cold Regions Heat Transfer*. ASME, New York (1987).
9. W. Aung and Y. Yener, Research directions in natural convection. In *Natural Convection Fundamentals and Applications* (Edited by S. Kakac *et al.*), pp. 1155–1171. Hemisphere, Washington, DC (1985).
10. M. A. Combarnous and S. A. Bories, Hydrothermal convection in saturated porous media. In *Advances in Hydroscience*, Vol. 10, pp. 231–307. Academic Press, New York (1976).
11. P. Cheng, Heat transfer in geothermal systems. In *Advances in Heat Transfer* (Edited by T. F. Irvine, Jr. and J. P. Hartnett), Vol. 14, pp. 1–106. Academic Press, New York (1978).
12. M. E. Goldstein and R. L. Reid, Effect of fluid flow on freezing and thawing of saturated porous media, *Proc. R. Soc. London* **365A**, 45–73 (1978).
13. A. R. Jumikis, Electrical thawing of frozen soils. In *Final Proc. Fourth Int. Conf. on Permafrost*, pp. 333–338. National Academy of Sciences Press, Washington, DC (1983).
14. T. V. Hromadka, II, G. L. Guymon and R. L. Berg, Comparison of two-dimensional domain and boundary integral geothermal models with embankment freeze–thaw field data. In *Final Proc. Fourth Int. Conf. on Permafrost*, pp. 509–513. National Academy of Sciences Press, Washington, DC (1983).
15. J. A. Weaver and R. Viskanta, Melting of liquid-saturated porous media, *Int. J. Heat Mass Transfer* **29**, 1943–1951 (1986).
16. M. Okada and T. Fukamoto, melting around a horizontal pipe embedded in a porous medium, *Trans. Japan Soc. Mech. Engrs* **48B**, 2041–2049 (1982).
17. C. Beckermann and R. Viskanta, Natural convection solid/liquid phase change in porous media, *Int. J. Heat Mass Transfer* **31**, 35–46 (1988).
18. S. Chellaiah, An experimental and numerical investigation of solid/liquid phase change of water saturated porous media in the presence of natural convection, Ph.D. Thesis, Purdue University, West Lafayette, Indiana (1988).
19. B. Gebhart and J. C. Mollendorf, Buoyancy-induced flows in water under conditions in which density-extrema may arise, *J. Fluid Mech.* **89**, 673–707 (1978).
20. T. H. Nguyen, P. Vasseur and L. Robillard, Natural convection between horizontal concentric cylinders with density inversion of water for low Rayleigh numbers, *Int. J. Heat Mass Transfer* **25**, 1559–1568 (1982).
21. B. Gebhart, Y. Jaluria, R. L. Mahajan and B. Sammakia, *Buoyancy-induced Flows and Transport*. Hemisphere, Washington, DC (1978).
22. A. K. Veinberg, Permeability, electrical conductivity, dielectric constant and thermal conductivity of a medium with spherical and ellipsoidal inclusions, *Soviet Physica Dokl.* **11**, 593–595 (1967).
23. W. Lindemann, Experimental and theoretical studies on design and calculations for latent heat storage, M.S.M.E. Thesis, Purdue University, West Lafayette, Indiana (1986).
24. J. C. Ward, Turbulent flow in porous media, *J. Hydraul. Div. ASCE* **90**, 1–12 (1964).
25. S. V. Patankar, *Numerical Heat and Fluid Flow*. Hemisphere, Washington, DC (1980).
26. R. F. Benenati and C. B. Brosilow, Void fraction distribution in beds of spheres, *A.I.Ch.E. Jl* **8**, 359–361 (1962).
27. D. Poulikakos and A. Bejan, Unsteady natural convection in a porous layer, *Physics Fluids* **26**, 1183–1191 (1983).
28. R. C. Weast (Editor), *Handbook of Chemistry and Physics* (60th Edn), pp. E10, F5–F6, F449–F451, D210–D211. CRC Press, Cleveland, Ohio (1984).
29. R. Viskanta, Natural convection in melting and solidification. In *Natural Convection Fundamentals and Applications* (Edited by S. Kakac *et al.*), pp. 845–877. Hemisphere, Washington, DC (1985).
30. H. Inaba and N. Seki, An experimental study of transient heat transfer characteristics in a porous layer enclosed betweeen two opposing surfaces with different temperatures, *Int. J. Heat Mass Transfer* **24**, 1854–1857 (1981).
31. B. K. C. Chan, C. M. Ivey and J. M. Barry, Natural convection in enclosed porous media with rectangular boundaries, *J. Heat Transfer* **92**, 21–27 (1970).
32. B. W. Webb and R. Viskanta, Analysis of heat transfer during melting of a pure metal from an isothermal vertical wall, *Numer. Heat Transfer* **9**, 539–558 (1986).
33. B. C. Chandrasekara and D. Vortmeyer, Flow model for velocity distribution in fixed porous beds under isothermal conditions, *Wärme- und Stoffübertr.* **12**, 105–111 (1979).

CONVECTION NATURELLE PENDANT LA FUSION D'UN MILIEU POREUX

Résumé—On étudie expérimentalement et numériquement la fusion d'un système glace-milieu poreux (billes de verre) contenu dans une cellule rectangulaire pour examiner les effets de la convection naturelle et de l'inversion de densité de l'eau dans la région de fusion. Quand la surchauffe à travers la région liquide est petite, l'écoulement dans le milieu poreux est faible et l'interface est plutôt plan. Pour de plus grandes surchauffes, l'intensité de la convection naturelle, la vitesse et la forme de l'interface dépendent de la différence de température imposée et de la perméabilité du milieu poreux. Les distributions mesurées de température sont comparées aux prédictions d'un modèle numérique qui considère à la fois la conduction dans le solide et la convection naturelle dans les régions liquides. Le modèle est basé sur la moyenne volumétrique des équations de transport, avec un changement de phase supposé se faire volumétriquement sur un petit domaine de température. On ajoute aux équations de Darcy, les extensions de Brinkman et Forchheimer. L'effet de l'inversion de densité de l'eau est modélisé. On trouve un accord raisonnablement bon entre les résultats de l'expérience et du calcul. Ces résultats établissent que la convection naturelle dans la région de fusion conduit à une forme non planaire du front et qu'elle accroît la vitesse de fusion.

SCHMELZEN DURCH NATÜRLICHE KONVEKTION IN EINEM GEFRORENEN PORÖSEN MEDIUM

Zusammenfassung—Das Schmelzen von Eis in einem porösen Medium (Glasperlen) in einer rechteckigen Testzelle wurde sowohl experimentell als auch numerisch untersucht, um den Einfluß der natürlichen Konvektion und der Dichteinversion bei Wasser in der Schmelzregion zu untersuchen. Ist die Überhitzung im Bereich der Flüssigkeit klein, so entsteht nur eine schwache Strömung im porösen Medium, und die Grenzfläche bleibt nahezu eben. Bei stärkerer Überhitzung hängt die Stärke des Konvektionsstroms, die Grenzflächengeschwindigkeit und deren Form maßgeblich von der Höhe der Temperaturdifferenz und der Durchlässigkeit des porösen Mediums ab. Die gemessenen Temperaturverteilungen werden mit den Vorhersagen aus dem numerischen Modell verglichen, das sowohl Wärmeleitung im Festkörper als auch natürliche Konvektion in der Flüssigkeit berücksichtigt. Das Modell basiert auf einer volumetrischen Mittelung der makroskopischen Transportgleichungen mit Phasenwechsel, der als volumetrisch über einen kleinen Temperaturbereich angenommen wird. Sowohl Brinkman- als auch Forchheimer-Beziehungen werden in die Darcy-Gleichungen eingebaut; die Dichteinversion von Wasser wird berücksichtigt. Es wird eine gute Übereinstimmung zwischen den experimentellen Werten und der numerischen Vorhersage erreicht. Abschließend läßt sich sagen, daß natürliche Konvektion in einem Schmelzbereich die Grenzflächenform beeinflußt und die Schmelzrate erhöht.

ТАЯНИЕ ЗАМОРОЖЕННОЙ ПОРИСТОЙ СРЕДЫ ЗА СЧЕТ ЕСТЕСТВЕННОЙ КОНВЕКЦИИ

Аннотация—Таяние системы лед–пористая среда (стеклянные шарики) в прямоугольной опытной ячейке исследовалось экспериментально и численно для выяснения эффектов естественной конвекции и инверсии в температурной зависимости плотности воды вблизи области плавления. При небольшом значении перегрева поперек жидкой области течение в пористой среде слабое, и граница раздела почти плоская. Найдено, что при более сильных перегревах интенсивность естественноконвективного течения, скорость перемещения границы раздела и ее профиль зависят от приложенной разности температур и от проницаемости пористой среды. Измеренные значения распределений температуры сравниваются с результатами расчетов по численной модели, в которой учитывается как теплопроводность твердого тела, так и конвекция в жидких областях. Модель основана на объемном осреднении уравнений макроскопического переноса в предположении, что фазовый переход происходит во всем объеме в небольшом диапазоне температур. Уравнения Дарси дополнены членами, учитывающими эффекты Бринкмана и Форщхаймера. Моделируется влияние инверсии плотности воды на течение жидкости и теплоперенос. Получено довольно хорошее совпадение между экспериментальными данными и результатами численных расчетов. Достоверно установлено, что из-за естественной конвекции в области плавления форма фронта становится неплоской и интенсивность таяния возрастает.